




# Sandwich-structured flexible strain sensors for gesture recognition in human–computer interaction

Guanzheng Chen<sup>1</sup>, Xin Zhang<sup>1</sup>, Zeng Sun<sup>1</sup>, Xuanzi Luo<sup>1</sup>, Guoqing Fang<sup>1</sup>, Huaping Wu<sup>2,a</sup>, Lin Cheng<sup>1,b</sup>, and Aiping Liu<sup>1,c</sup> 

<sup>1</sup> Zhejiang Key Laboratory of Quantum State Control and Optical Field Manipulation, Department of Physics, Zhejiang Sci-Tech University, Hangzhou 310018, China

<sup>2</sup> Key Laboratory of Special Purpose Equipment and Advanced Processing Technology, Ministry of Education and Zhejiang Province, College of Mechanical Engineering, Zhejiang University of Technology, Hangzhou 310023, China

Received 29 October 2024 / Accepted 27 February 2025

© The Author(s), under exclusive licence to EDP Sciences, Springer-Verlag GmbH Germany, part of Springer Nature 2025

**Abstract** Flexible strain sensors are crucial for advancing human–computer interaction (HCI) technologies, especially in applications that require precise and adaptive sensing capabilities. In this study, we use polydimethylsiloxane (PDMS) as the substrate material to construct sandwich-structured flexible strain sensors, incorporating a CNT/PDMS conductive polymer (CP) layer between two cross-positioned PDMS-transferred laser-induced graphene (LIG) strips (PL). The sandwich-structured PL/CP/PL sensor exhibits excellent flexibility, structural stability, and component compatibility, effectively enabling the detection of tensile, compressive, and bending strains while overcoming the limitations of single-layer strain sensors and facilitating the measurement of two-dimensional directional forces. Leveraging these capabilities, we apply the sensor to sign language recognition and develop a gesture-based HCI system that utilizes Morse and binary codes to enable intuitive, intelligent communication with the sensors. This advancement holds significant potential to enhance user experience and operational efficiency in virtual reality environments, coded communications systems, and robotics.

## 1 Introduction

Human–computer interaction (HCI) plays an increasingly pivotal role in contemporary scientific, technological, and engineering domains, with its fundamental objective being the attainment of efficient and friendly interactions between humans and computers to enhance work efficiency, improve the quality of life and foster scientific and technological innovation [1–4]. Currently, the development trajectory of HCI primarily encompasses multimodal interaction, intelligent interaction and sensor-free interaction, thereby imposing more stringent demands on sensor technology [5, 6]. Notably, flexible strain sensors serve as a crucial category within flexible sensors that monitor the surface deformation of objects. Consequently, they provide indispensable technical support for sensor applications in the field of HCI [7–11].

Numerous researchers have extensively investigated the material composition and structural design methodologies of novel flexible sensors to enhance both the sensitivity and strain detection range [12–14]. For instance, carbonaceous materials such as carbon nanotube (CNT) and graphene, along with metal nanomaterials like gold and silver nanowires exhibiting exceptional electrical conductivity, mechanical properties, and sensitivity have been employed as the sensing layer of piezoresistive flexible strain sensors [15–17]. Nevertheless, these conductive fillers possess inherent limitations in terms of stretchability and flexibility. To overcome this drawback, they are commonly combined with flexible matrices such as polydimethylsiloxane (PDMS), Ecoflex, and polyurethane (PU) to augment their sensing capabilities while maintaining good ductility [18, 19]. However, despite the simplicity in fabrication process mentioned above for these piezoresistive strain sensors, there is still room for improvement regarding

Guanzheng Chen and Xin Zhang contributed equally.

<sup>a</sup> e-mail: [wuhuaping@gmail.com](mailto:wuhuaping@gmail.com) (corresponding author)

<sup>b</sup> e-mail: [chenglin@zstu.edu.cn](mailto:chenglin@zstu.edu.cn) (corresponding author)

<sup>c</sup> e-mail: [liuaping1979@gmail.com](mailto:liuaping1979@gmail.com) (corresponding author)

their sensitivity due to their single-layer structure. Constructing various micro- and nanostructures (interlocking patterns, pyramidal arrays, pleated structures, etc.) on conductive films can also effectively improve the sensing performance of flexible strain sensors [20]. For example, Pang et al. utilized two interlocking high aspect ratio Pt-coated polymer nanofiber arrays supported on a thin PDMS layer to achieve the detection of weak physiological signals in humans [21]; Ge et al. prepared thick nanofolded graphene-elastomer sandwich structure through a rapid thermal annealing process, which significantly improved the sensitivity of the sensor and allowed the detection of subtle pressures [22]. Although the sensitivity is significantly improved compared to planar thin-film structures, the fabrication of microstructures requires silicon microtemplates or biomaterials, which results in higher material costs and susceptibility to damage during the demolding process. Moreover, sensors with microstructures experience a significant decrease in sensitivity under large strains. Introducing a spacer layer between two sensing layers can effectively broaden the sensing capability of the sensor and address the insensitivity issue of a single sensing layer towards vertical strain [23, 24]. For example, Huang et al. prepared thermoplastic polyurethane (TPU)/multi-walled carbon nanotubes (MWCNTs) nanocomposite foams with a multilayer alternating bimodal lattice structure by using a layer-by-layer hot pressing and supercritical carbon dioxide intermittent foaming process, which achieved a wide detection range, high sensitivity, and a low response time [25]. Fu et al. employed a layer-by-layer assembling technique to combine a two-dimensional (2D)  $\text{Ti}_3\text{C}_2\text{F}_x$  and MWCNTs nanocomposite foams with a sandwich stack structure, achieving high sensitivity and wide detection range [26]. The sandwich strain sensor developed by Tian et al. comprised a micro-spacer core layer of polystyrene microspheres sandwiched between two layers of laser-induced graphene (LIG/PU) film, demonstrating exceptional sensitivity, good linearity, wide sensing range, and excellent stability [27]. Obviously, the innovative sandwich structures effectively address the challenges faced by piezoresistive strain sensors in terms of high-pressure response and wide detection range. However, conventional flexible strain sensors with a similar sandwich structure are typically limited to detecting unidirectional strains and often encounter issues related to electrical connections between the upper, middle, and lower layers of the structure, which hinders their application in smart wearable devices and human–computer interaction.

Herein, a sandwich-structured piezoresistive flexible strain sensor was constructed by incorporating a CNT/PDMS (abbreviated as CP) intermediate layer between two transferred PDMS/LIG (abbreviated as PL) layers. Due to the utilization of PDMS and conductive carbon material in a cross-shaped assembly across its upper, middle, and lower layers, the sandwich-structured sensor exhibits excellent structural stability, interfacial cohesiveness, and electrical connectivity. The wearable placement of these flexible strain sensors on finger joints enables effective sign language recognition. The developed Morse decoding and binary coding system based on sandwich-structured flexible strain sensors offers intelligent and adaptive HCI applications that enhance user experience and operational efficiency in virtual reality, augmented reality, and robotic technology (Fig. 1). This advancement is expected to have significant implications in healthcare, entertainment industry as well as virtual reality and robotics fields.

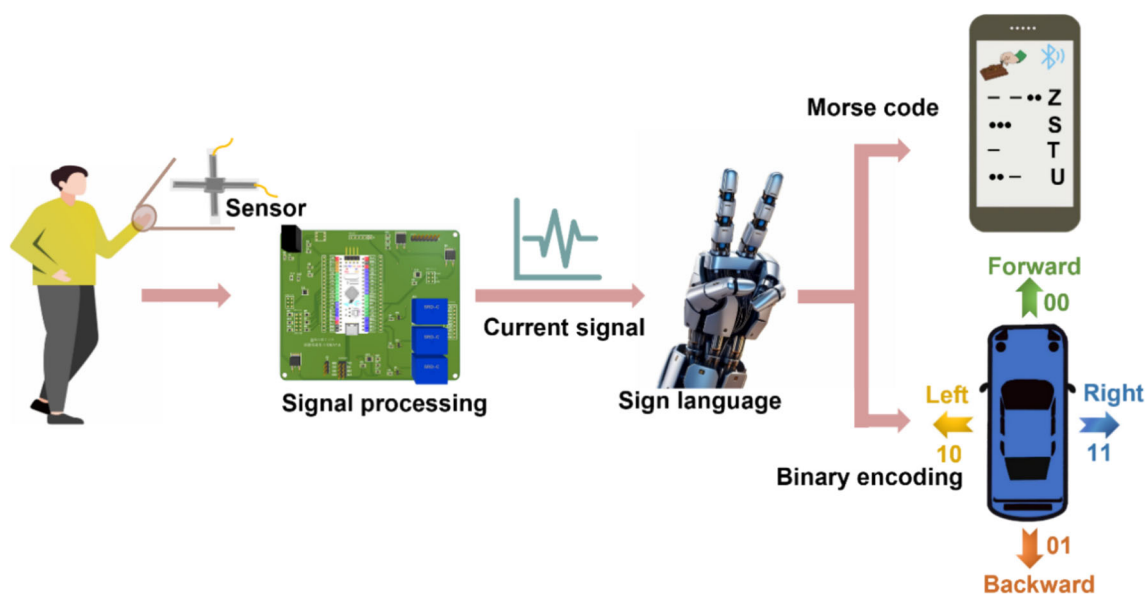


**Fig. 1** Schematic diagram of sandwich-structured flexible strain sensors for gesture recognition in HCI applications

## 2 Experimental section

### 2.1 Synthesis of PDMS/LIG

LIG was fabricated on a 0.05 mm thick polyimide (PI) film using a carbon dioxide laser (JTTS-ER, Harbin Jintai Laser Technology Co., Ltd.). The laser scanning speed was set at 100 mm/min, with a frequency of 20 kHz and power output of 3.2 W. A CAD software was employed to design the laser path, with the central square measuring  $0.8 \times 0.8 \text{ cm}^2$  and the two side strips measuring  $0.2 \times 0.9 \text{ cm}^2$  in dimensions. Subsequently, an appropriate amount of PDMS mixed with curing agent was mixed evenly and applied onto the LIG surface, followed by vacuum treatment in a constant temperature dryer (FD-1A-80, Shanghai Li wen Scientific Instrument Co., Ltd.) to ensure thorough penetration of the sticky PDMS into the 3D porous structure of LIG. The sample was then transferred to a convection oven (DZF-6030A, Shanghai Jing hong Experimental Equipment Co., Ltd.) for cross-linking at  $80^\circ\text{C}$  for 1 h. After complete curing, the PDMS/LIG (PL) layer was peeled off from the PI film and copper wires were connected at both ends using conductive silver paste (Fig. S1).

### 2.2 Fabrication of the sandwich-structured flexible strain sensors

A strip of PL obtained above was placed under a custom cross-shaped mold ( $1 \times 1 \text{ cm}^2$  square in the middle of the cross,  $0.3 \times 0.8 \text{ cm}^2$  strips on both sides). Then a mixture of CNTs and PDMS ( $W_{\text{CNTs}}:W_{\text{PDMS}} = 7\%:93\%$ ) was poured into the cross-shaped mold, followed by placing another strip of PL perpendicular to the lower PL strip on the upper layer of the CP. The sandwich-structured PL/CP/PL material was subjected to curing at  $80^\circ\text{C}$  for 3 h in a convection oven. After complete curing, the mold was removed, and a flexible strain sensor with a sandwich structure was obtained (Figs. S1 and S2).

### 2.3 Measurement and characterization

The morphological characteristics of the PL and CP were meticulously examined using a field-emission scanning electron microscope (FESEM S-4800, Hitachi, Japan), operating at a low acceleration voltage of 3 kV to preserve sample integrity. Raman spectroscopy (LabRAM HR Evolution, HORIBA France SAS) was employed for analyzing the composition and structural characteristics of PL and CP layers. The force and electricity test were performed using a mechanical testing machine (HY-0230, Yi heng Precision Instruments). The resistance changes exhibited by the flexible sandwich-structured sensor under different test conditions were collected using a synchronous AD acquisition card (USB\_HRF4028, Heng rui feng Measurement and Control Technology Co., Ltd.).

## 3 Results and discussion

### 3.1 Microstructure of sensor

For the upper and lower PL layers, LIG is chosen as the preferred material for flexible sensors due to its excellent electrical conductivity, remarkable strain sensitivity properties, and cost-effectiveness [28–30]. The SEM image in Fig. 2a reveals that the grooves generated during the laser-induced preparation of LIG are still clearly visible, and the porous foam structure of LIG is retained after transferred onto PDMS (Fig. 2d). Moreover, PDMS filled into the porous structure of LIG plays a supportive role in enhancing the flexibility and tensile properties of LIG, and the PL exhibited excellent structural stability (Fig. S3) and electrical signal stability (Fig. S4). For the CP elastomer, as shown in Fig. 2b, the CNTs are uniformly dispersed within the PDMS to ensure the continuous electrical conduction through CP (Fig. 2e). In addition, the cross-sectional SEM image in Fig. S5 also clearly shows the close connection between the PDMS, LIG and CP layers within the sensor. The Raman spectrum of PL shows three distinct characteristic peaks of graphene (Fig. 2c): the D peak at  $1350 \text{ cm}^{-1}$  is the disordered vibration peak of graphene; the G peak near  $1590 \text{ cm}^{-1}$  comes from the first-order  $E_{2g}$  phonon planar vibration; the 2D peak near  $2670 \text{ cm}^{-1}$  is the second-order Raman peak of two-photon resonance [31]. The intensity ratio ( $I_D/I_G$ ) is 0.4, indicating that the corresponding LIG has fewer defects with high degree of graphitization. The Raman spectrum of CP (Fig. 2f) shows three distinct CNT characteristic peaks (D, G and 2D) associated with CNTs, where the frequency of the 2D peak is approximately twice that of the D peak [32]. In addition, both Raman spectra presented in Figs. 2c, f exhibit characteristic peaks associated with PDMS at  $2905 \text{ cm}^{-1}$  and  $2964 \text{ cm}^{-1}$  [33, 34].

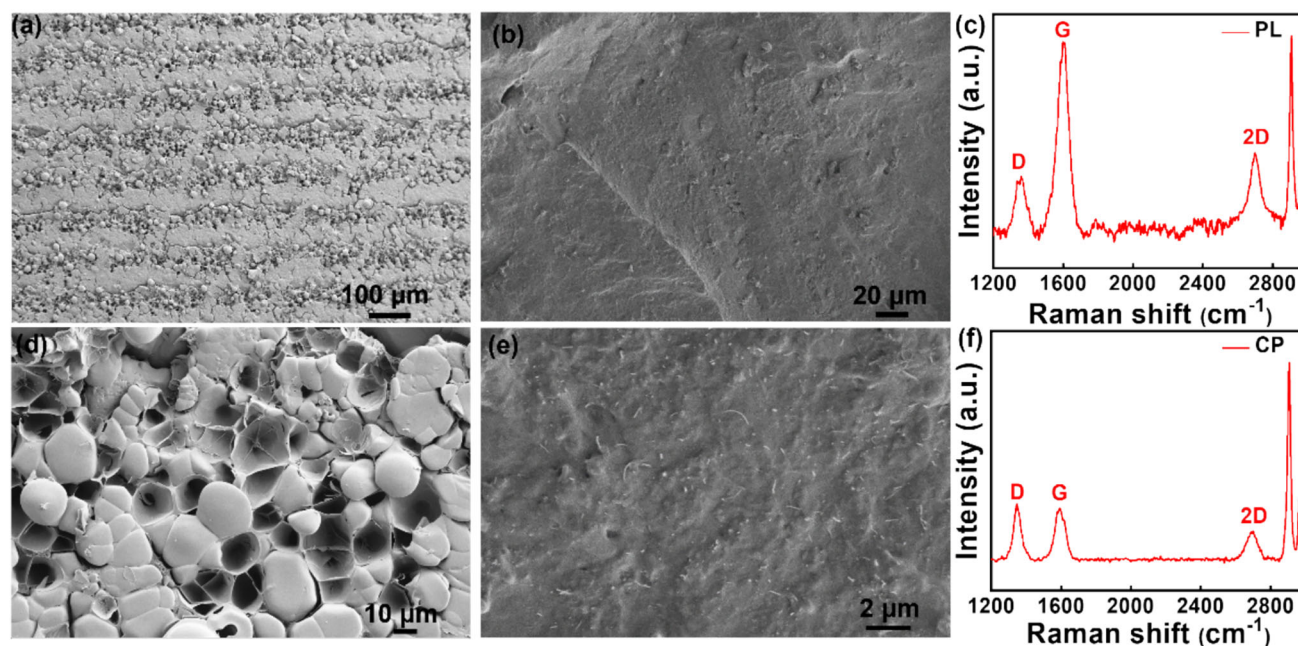


**Fig. 2** Characterization of PL and CP layers. **a** and **d** SEM images of PL layer at different magnifications, **b** and **e** SEM images of CP layer at different magnifications, **c** Raman diagram of PL layer, **f** Raman diagram of CP layer

### 3.2 Sensing performance

The special cross-shaped structure design of flexible strain sensors allows them to be stretched not only along the X-axis but also along the Y-axis (Fig. S6). When the PL layer is subjected to uniaxial stretching, a large number of microcracks are usually generated in both the upper and lower layers of the PL layer, resulting in the formation of island-shaped conductive areas (Fig. 3a). This leads to a significant reduction or even breakage of the conductive paths and a sudden increase in the conductive resistance [35]. As shown in Fig. 3e, the electrical signal response of sandwich-structured flexible strain transducer shows an approximately linear relationship in the range of 0–20% tensile strain, with a sensitivity GF of 17.8. The black curve illustrates the change in the electrical signal when simultaneously stretched along both axes, showing a similar resistance increase trend as observed during uniaxial stretching along the X-axis (red curve in Fig. 3e). Notably, the maximum error is less than 6%, which indicates minimal influence from other axes during uniaxial stretching and confirms its ability to detect external stimuli from different directions in a two-dimensional manner. However, in the case of the single-layer PL strain sensor, the resistance exhibits a sharp increase to an infinite value when subjected to only 10% strain due to a significant reduction in the conductive pathway (Fig. S7a). Additionally, the sandwich-structured flexible strain exhibits a remarkable response capability with rapid response and recovery times of 40 ms and 85 ms to external stimuli, respectively (Fig. S7b), indicating its excellent strain responsiveness. Another distinguishing feature of sandwich-structured flexible strain sensors from uniaxial tensile PL sensors is their significantly increased compressibility. As shown in Fig. 3h, the resistance of the sensor gradually increases with increasing pressure. When a pressure of 250 kPa is applied, the relative resistance of the sensor undergoes an approximate 100% change. The linearity of the sensor is very good over the pressure range of 0–250 kPa with a GF value of 0.0039 (Fig. 3h), surpassing that observed for upper/lower PL monolayer and CP interlayer counterparts. This superiority can be attributed to increased cracks in the LIG on the PL strip under compression (Fig. 3b), leading to an elevation in resistance. Simultaneously, the CP layer undergoes horizontal expansion during vertical compression, which leads to a significant reduction in the conduction path (Fig. 3d) [36].

The sandwich-structured flexible strain sensors exhibit exceptional tensile and compressive characteristics, as well as remarkable bending deformation sensing capabilities. Within the bending range of 0°–120°, the resistance demonstrates a linear variation with a GF value of 0.0116 (Fig. 3k). This can be attributed to the reverse bending experienced by the upper layer of PL and forward bending undergone by the lower layer (Fig. 3c). Forward bending results in LIG breakage, while reverse bending has minimal impact on LIG connectivity (Fig. 3k). The change in resistance is more pronounced in the forward-bending PL layer PL compared to that in the reverse-bending PL layer, both exhibiting an increasing trend (Fig. 3k). Furthermore, there is a decrease in surface density of CNTs within the intermediate CP layer (Fig. 3d), leading to an increase in resistance [37]. For bending experiments at different angles in the range of 0–90° the relative resistance change of the sensor also shows a step-type change, and



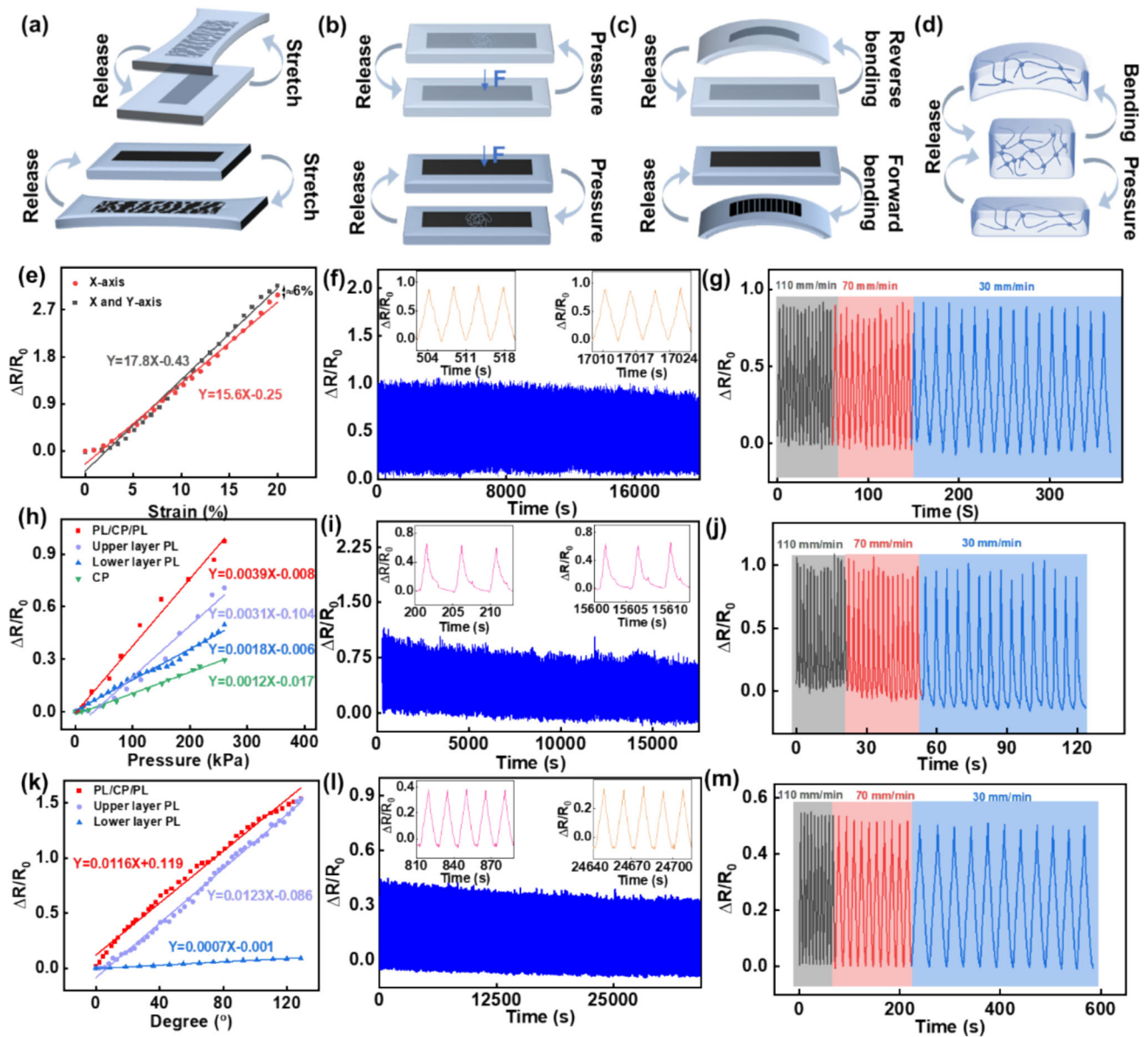


**Fig. 3** Mechanical analysis and electromechanical testing of sandwich-structured flexible strain sensors. Schematic deformation mechanisms of **a** uniaxial stretching process, **b** compression process of upper and lower PL layers in the sandwich structure, and **c** forward bending and reverse bending process. **d** Compression and bending process of CP layer. Changes in the relative resistance of the sandwich-structured flexible strain sensors under tension: **e** uniaxial stretching along the X-axis and simultaneous stretching along the X-axis and Y-axis with fixing the Y-axis at 20% strain, **f** cyclic stretching up to 8% strain for 4000 times, and **g** cyclic stretching up to 8% strain at different frequencies. The relative resistance changes of sandwich-structured flexible strain sensors and partial monolayer structure under pressure: **h** linear pressure increase up to 250 kPa, **i** cyclic pressure up to 200 kPa for 4000 cycles, and **j** cyclic pressure up to 200 kPa at different frequencies. The relative resistance changes of sandwich-structured flexible strain sensors and partial monolayer structure under bending action: **k** cyclic bending up to 120°, **l** cyclic bending up to 30° for 2500 times, and **m** cyclic bending up to 45° at different frequencies

the electrical signal can be well maintained after bending (Fig. S8). The sandwich-structured flexible sensors are also subjected to durability assessment, and their fatigue resistances are evaluated through 4000, 4000 and 2500 loading and unloading cycles under tension, compression, and bending conditions (Fig. 3f, i, l). Enlarged plots in the inset depict the sustained service life and stability of the sensors over thousands of tensile, compressive, and bending cycles by illustrating changes in electrical signals during cycling. Furthermore, it is observed that the alterations in electrical signals generated by the sensor during tensile, compressive, and bending deformation remain unaffected by variations in loading frequency (Fig. 3g, j, m). Moreover, we tested the resistance change of the sandwich-structured flexible strain sensor as the temperature increased from 20 to 60 °C (Fig. S9). In practical applications, the ambient temperature generally does not exceed 40 °C, and the corresponding resistance change of the sensor is kept below 0.04. The temperature induced changes are negligible compared to the strain related signal changes, proving the good environmental stability of the sensor.

### 3.3 Application of sandwich-structured flexible strain sensors in sign language recognition

As a structured language, sign language conveys semantic information through hand shape, direction, arm movements and facial expressions [38]. Sign language is more convenient and flexible than written language, and has become the simplest and most direct means of communication between individuals who are deaf or mute [39]. However, due to the lack of systematic learning and usage of sign language among the general population, effective communication with individuals who are deaf or mute becomes challenging, resulting in various inconveniences in their work and daily lives.

Considering that finger bending typically falls within the range of a 90° angle, the corresponding strain remains within 8%. Thus, based on the linear range of tensile, compressive, and bending deformations depicted in Fig. 3, this sensor can be comfortably worn on the finger to effectively illustrate the relationship between electrical signals and deformation during finger movement. This enables us to establish an internal correlation between finger motion and electrical signals. Flexible wearable sensors can be directly attached to the human hand or integrated into wearable gloves to enable real-time gesture recognition and conversion into text or voice output, thus establishing a barrier-free communication bridge between individuals who are deaf or mute and those without hearing impairments. Gesture recognition based on flexible wearable sensors has also been widely used in rehabilitation medicine, smart homes, control of high-tech electronic devices and virtual systems thus playing an increasingly important role in the field of HCI [40–42].

We affixed the prepared sandwich-structured flexible strain sensor onto the second joints of all five fingers (Fig. 4a), connected it to a 5-channel AD acquisition card, and recorded the variations in electrical signals during finger movements. When transitioning to sign language number "6", with only the thumb and little finger extend while others bend, the electrical signal remain stable near its initial resistance value for these two fingers but increase synchronously for the remaining three (Fig. 4b). When transitioning to sign language number "8", with only the thumb and mouth feed extend while others bend, the electrical signal remain stable near its initial resistance value for these two fingers but increase synchronously for the remaining three (Fig. 4c). Similarly, when switching to sign language numbers "1" and "0" (Figs. S10a and S10b), real-time changes in electrical signals are detected for bent fingers (step-shaped relative resistance increase) and straightened fingers (smooth straight line). In addition, the gestures representing "Good" (Fig. S10c) and "OK" (Fig. 4d) in sign language are also tested. These findings further verify the feasibility and advantages of our sandwich-structured flexible strain sensor in gesture recognition, facilitating seamless communication between individuals who are deaf or mute and those unfamiliar with sign language.

### 3.4 Morse decoding interaction system based on sandwich-structured flexible strain sensor

To further validate the feasibility of the sandwich-structured flexible strain sensor in HCI, we affixed the sensor to a finger as a telegraph generator (Fig. 5a). The duration of finger bending during telegraphy was utilized to differentiate between dahs and dots specified in international Morse code (Fig. 5b), followed by communication using Morse encryption codes (Fig. 5a). For instance, when encoding "Hello" in Morse code, it is observed that the letter "H" corresponds to four dots (four rapid bending movement of the finger), generating four distinct electrical signals with sharp characteristics (Fig. 5a). Similarly, the letter "E" is represented by one dot, which corresponds to a quick bend of the finger; while for the letter "L", it consists of one dot followed by one dah and then two dots—thus, during dot formation, there is a rapid bending and recovery motion of the finger whereas for dah formation, continuous bending is maintained. A rapid increase in electrical signal amplitude, then stable electrical signals, followed by relative resistance return to its initial value corresponds to a complete process of finger bending, maintain and straightening (Fig. 5a). By conducting these experiments on sensors corresponding to Morse codes such as "HANG," "ZHOU," and "THANKS" (Fig. 5c–e), we confirm that our flexible strain sensor can effectively serve as a telegraph generator for Morse encoding.

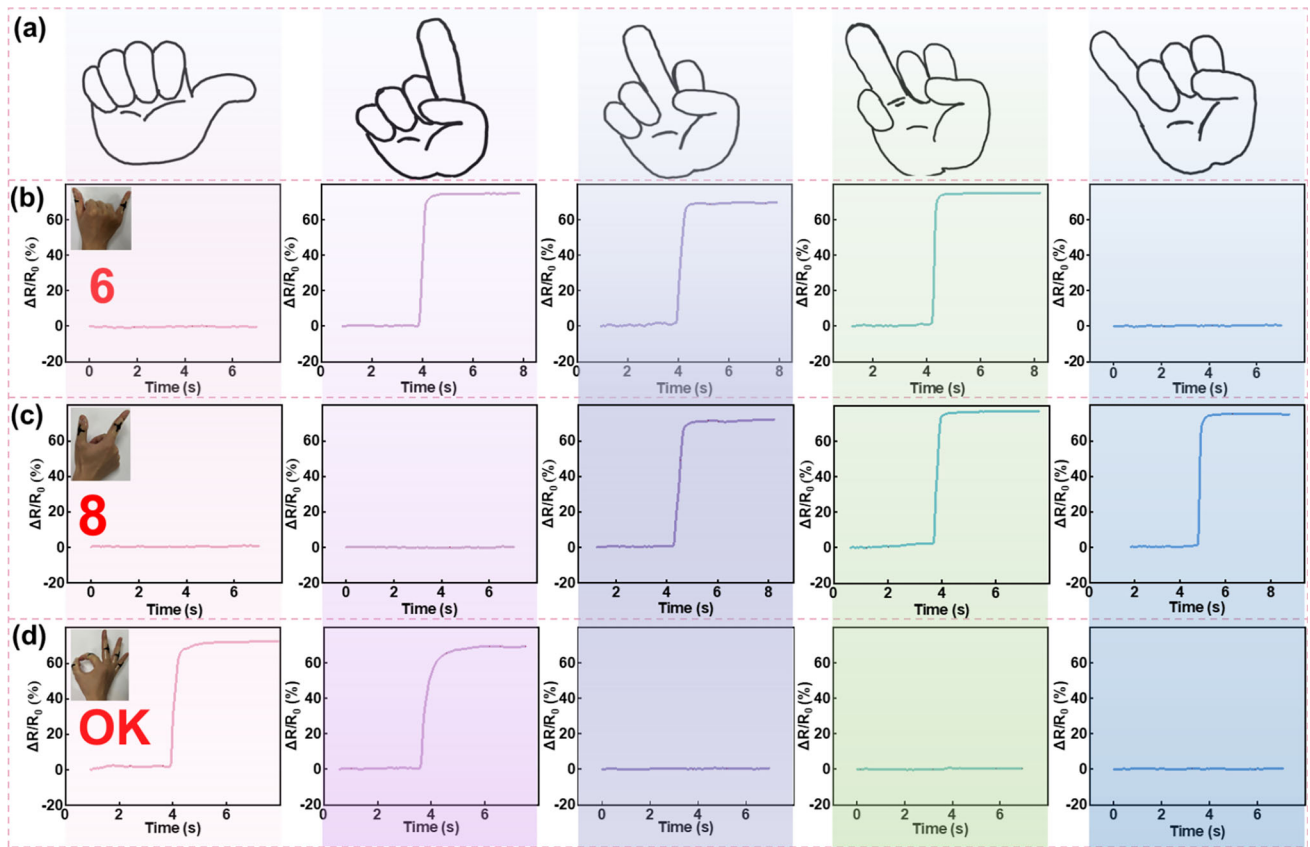


**Fig. 4** a Schematic diagram of five fingers. b, c and d Real-time electrical signal changes of five sandwich-structured flexible strain sensors worn on the fingers when performing the gestures of "6", "8" and "OK" in sign language

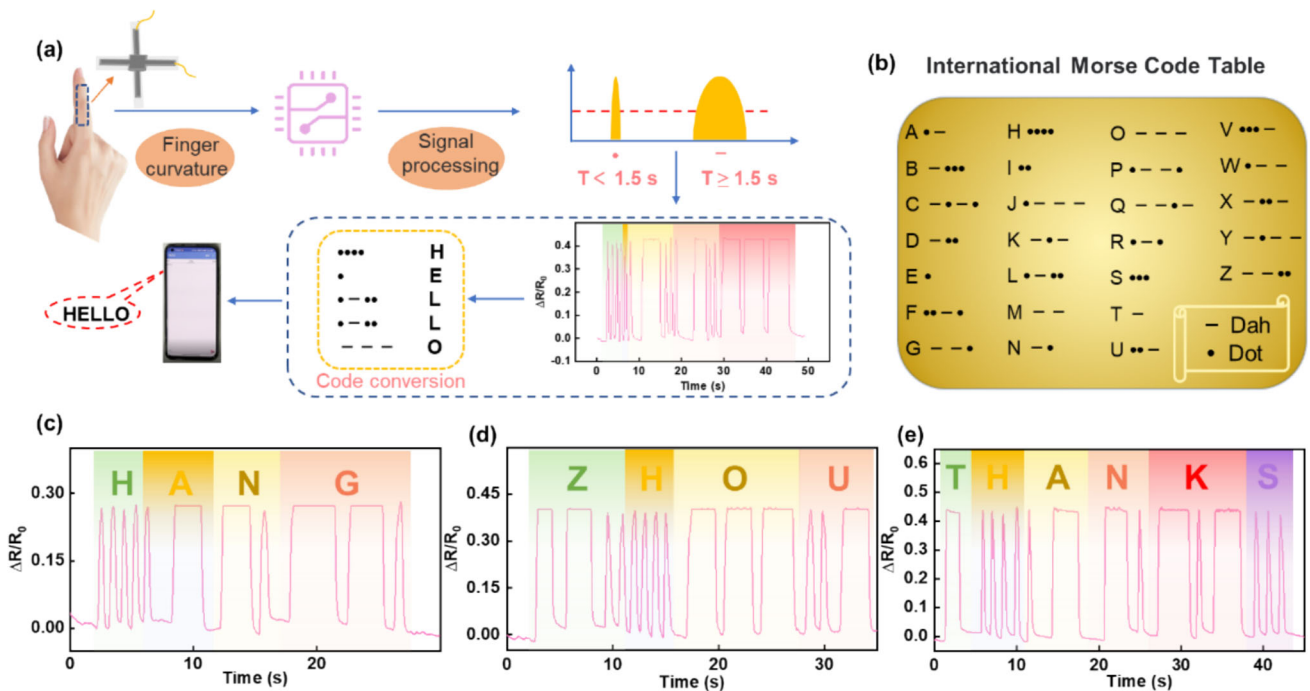


**Fig. 5** Morse decoding interaction system based on sandwich-structured flexible strain sensor. a Schematic flow diagram of the Morse decoding system based on a sandwich-structured flexible strain sensor. b Morse code table corresponding to the 26 letters of the alphabet. c, d, and e Relative resistance change when sending Morse codes "HANG", "ZHOU" and "THANKS" with a sandwich-structured flexible strain sensor worn on the finger as a telegraph generator

Based on this premise, a HCI system is developed for Morse code decoding using the sandwich-structured flexible strain sensor affixed to the joint of the index finger (Figs. S11 and S12a) and signal acquisition is performed by a single-chip microcomputer (GD32E230C8T6). The signal processing module employs logical judgment to accommodate human reaction time. A signal recording occurs when the finger bends, followed by another recording after 1.5 s elapsed. If it is determined that the finger has bent again, it represents a stroke; otherwise, it indicates a dot (Figs. S12b, c). Subsequently, Morse code signals are decoded and transmitted wirelessly via Bluetooth to a mobile phone (Fig. 5a). Supplementary movies 1–3 demonstrate real-time display of encoding processes such as dots and dahs on an LCD screen of the microcontroller when utilizing the sensor-equipped finger as a telegraph generator; ultimately resulting in accurate letter decoding and display. Evidently, this HCI system development based on the low-cost flexible strain sensor offers accessibility without barriers thus serving as an auxiliary communication technology for individuals with disabilities by enhancing their communicative abilities to some extent. This provides an alternative and convenient input method, thereby opening up new possibilities for HCI applications across diverse scenarios.

### 3.5 Binary coding interaction system based on sandwich-structured flexible strain sensor

As an important medium in the digital information era, binary code solely comprises ‘0’ and ‘1’ two signal states, exhibiting uncomplicated technical implementation, straightforward arithmetic rules, suitability for logical operations, ease of conversion, and robust anti-interference capabilities. Consequently, binary has emerged as the optimal choice for computer-based information storage and processing. In terms of HCI, computers and intelligent devices often necessitate algorithmic processing of received control signals followed by their conversion into operable binary codes by the controller. This significantly augments interaction time. Moreover, complex signal recognition poses challenges to HCI implementation; however, this can be circumvented through direct binary coding utilizing flexible wearable strain sensors to execute simple mechanical control operations (Fig. 6a).

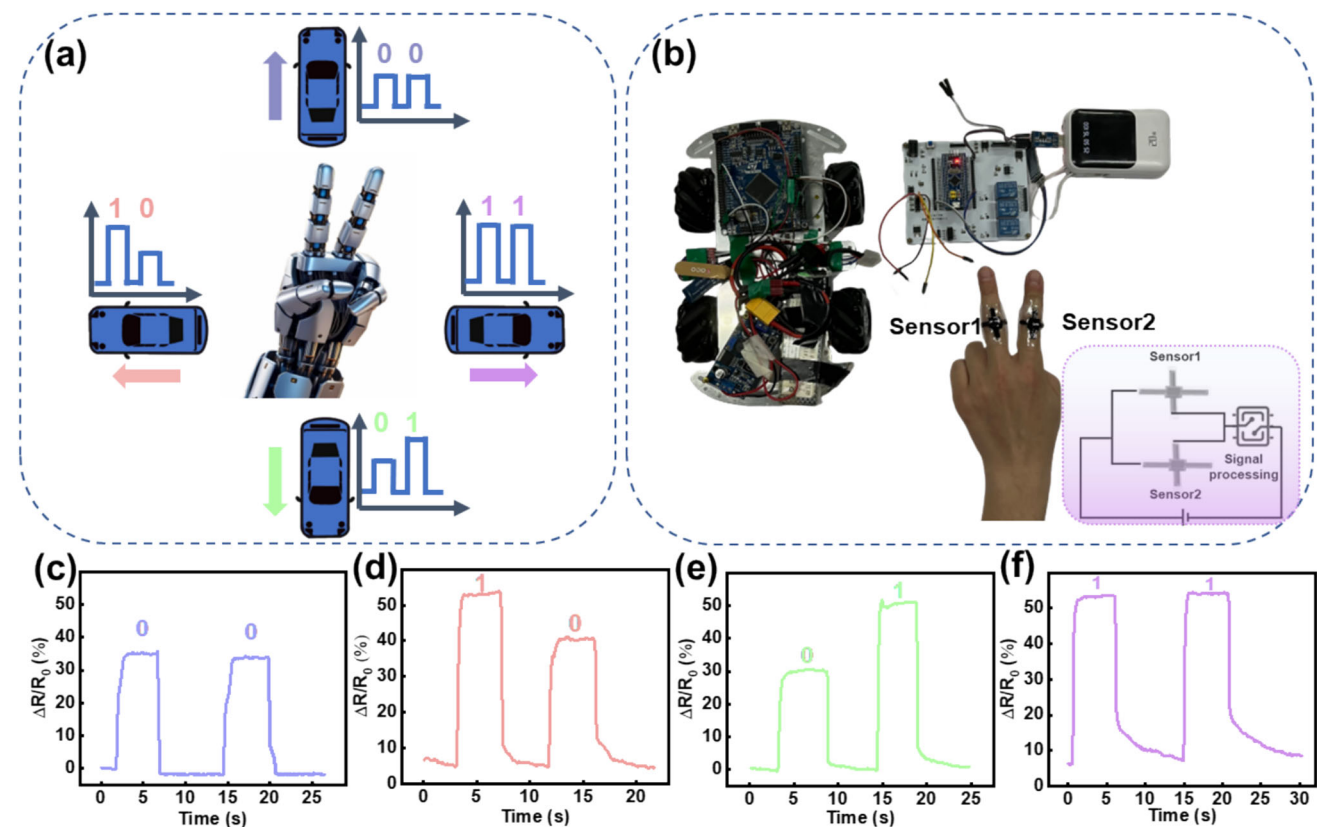


**Fig. 6** Binary coding interaction system based on a sandwich-structured flexible strain sensor. **a** Schematic illustration of the rule definition of the binary coding interaction system based on a sandwich-structured flexible strain sensor. **b** Optical diagram of two sandwich-structured flexible strain sensors worn on the finger for binary-coded control of cart motion (the inset shows the corresponding parallel circuit principle). **c–f** Relative resistance changes of sandwich-structured flexible strain sensors during binary variable coding



By connecting two sensors in parallel to the index and middle fingers (inset of Fig. 6b), the bending of either finger can lead to an increase in the resistance value across the parallel resistor, with a larger resistance increase observed when both fingers are bent simultaneously. The resistance of the parallel circuit is defined as "1" when two fingers are bent together, and as "0" when only one finger is bent. The relative changes in resistance values corresponding to finger movements "00", "01", "10", and "11" are depicted in Fig. 6c–f, enabling clear differentiation between different movement patterns. A binary coding interaction system assigns the received signals of "00" for forward motion, "01" for backward motion, "10" for left turn, and "11" for right turn (Figs. 6a and S13). Movie 4 demonstrates how this parallel flexible sensor enables control over the motion of a smart cart. Furthermore, considering its programmability, only three-bit binary encoding is required to control finger movement three times and achieve eight distinct forms of movement thus highlighting its promising application prospects in robot motion control scenarios requiring programmable capabilities.

## 4 Conclusion

The sandwich-structured flexible strain sensor was fabricated by incorporating a CNT/PDMS conductive polymer (CP) layer sandwiched between two layers of cross-aligned PDMS-transferred laser-induced graphene (PL) strips. This peculiar sandwich structure overcomes the limitations of single-layer strain sensors in detecting pressure-induced strains. Moreover, due to its cross-shaped combination design, it exhibits remarkable capability in sensing two-dimensional directional forces. Considering its outstanding sensing performance under tensile, compressive, and bending strains, we employ this sensor for sign language recognition and develop a HCI system based on Morse code and binary code. Our work showcases the significance of this technology in enhancing user experience and operation in various fields such as virtual reality, coded communication, and robotics.

**Supplementary Information** The online version contains supplementary material available at <https://doi.org/10.1140/epjs/s11734-025-01560-9>.

**Acknowledgements** This work was supported by the National Natural Science Foundation of China (No. 12272351, 62401509 and 12372168), the Youth Top-notch Talent Project of Zhejiang Ten Thousand Plan of China (No. ZJWR0308010), the Zhejiang Provincial Natural Science Foundation of China (No. LZ24A020004 and LRG25A020001), the "Pioneer" and "Leading Goose" R&D Program of Zhejiang (Grant no. 2023C01051).

## Author contribution statement

GC: methodology, software, data curation, writing-original draft preparation; XZ: data curation, software, validation; ZS: software, validation; XL: software, validation; GF: formal analysis, investigation; HW: investigation; LC: investigation; AL: supervision.

**Data availability statement** Available on request.

## Declaration

**Conflict of interest** The authors declare that they have no known competing financial interests or personal relationships that could have appeared to influence the work reported in this paper.

## References

1. R.Y. Zhang, M. Hummelgard, J. Ortengren, M. Olsen, H. Andersson, Y. Yang, H. Olin, Z.L. Wang, Utilising the triboelectricity of the human body for human-computer interactions. *Nano Energy* **100**, 107503 (2022). <https://doi.org/10.1016/j.nanoen.2022.107503>
2. J. Li, C. Carlos, H. Zhou, J.J. Sui, Y.K. Wang, Z. Silva-Pedraza, F. Yang, Y.T. Dong, Z.Y. Zhang, T.A. Hacker, B. Liu, Y.C. Mao, X.D. Wang, Stretchable piezoelectric biocrystal thin films. *Nat. Commun.* **14**, 6562 (2023)
3. L. Cheng, G.Q. Fang, L. Wei, W.Z. Gao, X.E. Wang, Z.H. Lv, W.J. Xu, C. Ding, H.P. Wu, A.P. Liu, Laser-induced graphene strain sensor for conformable lip-reading recognition and human-machine interaction. *ACS Appl. Nano Mater.* **6**, 7290–7298 (2023). <https://doi.org/10.1021/acsanm.3c00410>
4. Y. Qiu, Y. Tian, S.S. Sun, J.H. Hu, Y.Y. Wang, Z. Zhang, A.P. Liu, H.Y. Cheng, W.Z. Gao, W.A. Zhang, H. Chai, H.P. Wu, Bioinspired, multifunctional dual-mode pressure sensors as electronic skin for decoding complex loading processes and human motions. *Nano Energy* **78**, 105337 (2020). <https://doi.org/10.1016/j.nanoen.2020.105337>

5. C. Ning, K. Dong, R.W. Cheng, J. Yi, C.Y. Ye, X. Peng, F.F. Sheng, Y. Jiang, Z.L. Wang, Flexible and stretchable fiber-shaped triboelectric nanogenerators for biomechanical monitoring and human-interactive sensing. *Adv. Funct. Mater.* **31**, 2006679 (2021). <https://doi.org/10.1002/adfm.202006679>
6. T.Y. Wang, C. Wang, Q.X. Zeng, G.Q. Gu, X. Wang, G. Cheng, Z.L. Du, A real-time, self-powered wireless pressure sensing system with efficient coupling energy harvester, sensing, and communication modules. *Nano Energy* **125**, 109533 (2024). <https://doi.org/10.1016/j.nanoen.2024.109533>
7. X. Wang, J. Yang, K.Y. Meng, Q. He, G.Q. Zhang, Z.H. Zhou, X.L. Tan, Z.P. Feng, C.C. Sun, J. Yang, Z.L. Wang, Enabling the unconstrained epidermal pulse wave monitoring via finger-touching. *Adv. Funct. Mater.* **31**, 2102378 (2021). <https://doi.org/10.1002/adfm.202102378>
8. Y. Qiu, F.N. Wang, Z. Zhang, K.Q. Shi, Y. Song, J.T. Lu, M.J. Xu, M.Y. Qian, W.A. Zhang, J.X. Wu, Z. Zhang, H. Chai, A.P. Liu, H.Q. Jiang, H.P. Wu, Quantitative softness and texture bimodal haptic sensors for robotic clinical feature identification and intelligent picking. *Sci. Adv.* **30**(10), 0348 (2024). <https://doi.org/10.1126/sciadv.adp0348>
9. S.P. Ji, P. Guo, D.Q. Ruan, H.P. Wu, L. Cheng, A.P. Liu, Flexible strain sensor with self-healing function for human motion monitoring. *Funct. Mater. Lett.* **16**(2), 2350010 (2023). <https://doi.org/10.1142/S1793604723500108>
10. C.J. Wan, G. Chen, Y.M. Fu, M. Wang, N. Matsuhisa, S.W. Pan, L. Pan, H. Yang, Q. Wan, L.Q. Zhu, X.D. Chen, An artificial sensory neuron with tactile perceptual learning. *Adv. Mater.* **30**, 1801291 (2018). <https://doi.org/10.1002/adma.201801291>
11. X.L. Chen, J.Y. Shao, H.M. Tian, X.M. Li, C.H. Wang, Y.S. Luo, S. Li, Scalable imprinting of flexible multiplexed sensor arrays with distributed piezoelectricity-enhanced micropillars for dynamic tactile sensing. *Adv. Mater. Technol.* **5**, 2000046 (2020). <https://doi.org/10.1002/admt.202000046>
12. Z.D. Li, F.M. Hu, Z.M. Chen, J.C. Huang, G.N. Chen, R.B. Chen, M.M. Wei, K. Lao, J.J. Hu, J.T. Zheng, L.F. Wang, Y. Yao, X.Y. Hu, B.W. Liang, M. Yang, X.H. Lu, J.X. Wen, J.Y. Luo, Fiber-junction design for directional bending sensors. *npj Flex Electron.* **5**, 4 (2021).
13. F. Li, H.J. Wang, S.Q. Nan, Y.P. Yang, Z.C. Wang, R. Zhu, T.W. Zhang, J. Zhang, Flexible pressure sensors tuned by interface structure design-numerical and experimental study. *Appl. Surf. Sci.* **638**, 158021 (2023). <https://doi.org/10.1016/j.apsusc.2023.158021>
14. J. Tang, C. Zhao, Q. Luo, Y. Chang, Z. G. Yang, T. R. Pan, Ultrahigh-transparency and pressure-sensitive iontronic device for tactile intelligence. *npj Flex Electron.* **6**, 54 (2022).
15. Y. Tian, J.K. Han, J.K. Yang, H.P. Wu, H. Bai, A highly sensitive graphene aerogel pressure sensor inspired by fluffy spider leg. *Adv. Mater. Interfaces* **8**, 2100511 (2021). <https://doi.org/10.1002/admi.202100511>
16. J. Tang, Y.T. Wu, S.D. Ma, T. Yan, Z.J. Pan, Flexible strain sensor based on CNT/TPU composite nanofiber yarn for smart sports bandage. *Compos Part B-Eng* **232**, 109605 (2022). <https://doi.org/10.1016/j.compositesb.2021.109605>
17. C.M. Qu, X. Yu, Y. Xu, S.C. Zhang, H.Y. Liu, Y.L. Zhang, K. Huang, L.F. Lv, A sensing and display system on wearable fabric based on patterned silver nanowires. *Nano Energy* **104**, 107965 (2022). <https://doi.org/10.1016/j.nanoen.2022.107965>
18. J.W. Chen, Y.T. Zhu, W. Jiang, A stretchable and transparent strain sensor based on sandwich-like PDMS/CNTs/PDMS composite containing an ultrathin conductive CNT layer. *Compos. Sci. Technol.* **186**, 107938 (2020). <https://doi.org/10.1016/j.compscitech.2019.107938>
19. L. Cheng, D.Q. Ruan, Y.W. He, J.Y. Yang, W. Qian, L.W. Zhu, P.D. Zhu, H.P. Wu, A.P. Liu, A highly stretchable and sensitive strain sensor for lip-reading extraction and speech recognition. *J. Mater. Chem. C* **11**, 8413–8422 (2023)
20. Z.H. Lv, L. Cheng, G.Z. Chen, X.Z. Luo, H. Yu, H.X. Zhang, H.P. Wu, A.P. Liu, Ionic flexible capacitive three-dimensional force sensor for electromechanical signal monitoring. *IEEE Sens. J.* **24**, 26309–26319 (2024)
21. C.H. Pang, G.Y. Lee, T. Kim, S.M. Kim, H.N. Kim, S.H. Ahn, K.Y. Suh, A flexible and highly sensitive strain-gauge sensor using reversible interlocking of nanofibers. *Nat. Mater.* **11**, 795–801 (2012)
22. Z. Hu, L.Q. Zhang, M.C. Wang, Flexible pressure sensor based on a thermally induced wrinkled graphene sandwich structure. *IEEE Sens. J.* **22**, 3040–3051 (2022)
23. X.H. Chang, L.R. Chen, J.W. Chen, Y.T. Zhu, Z.H. Guo, Advances in transparent and stretchable strain sensors. *Adv. Compos. Hybrid Mater.* **4**, 435–450 (2021)
24. Z. Sang, K. Ke, I. Manas-Zloczower, Interface design strategy for the fabrication of highly stretchable strain sensors. *ACS Appl. Mater. Interfaces* **10**, 36483–36492 (2018). <https://doi.org/10.1021/acsami.8b14573>
25. A. Huang, Y.W. Zhu, M.H. Zhou, B. Tan, Y. Song, G.X. Huang, H.Y. Huang, X.F. Peng, Lightweight, porous, stretchable nanocomposite foams with sandwich-like and bimodal cell structure by supercritical fluids-assisted processing for flexible strain sensor. *J. Supercrit. Fluids* **204**, 106112 (2024). <https://doi.org/10.1016/j.supflu.2023.106112>
26. X. Fu, H. Tong, Y.T. Wu, K. Zhang, X. Sheng, L. Douadji, G.T. He, Z.C. Qiu, B.P. Zhou, S. Kang, J.L. Luo, Z.W. Pan, W.Q. Lu, Flexible sensors with a sandwich stack structure of few-Layer  $\text{Ti}_3\text{C}_2\text{F}_x$ /polypyrrole nanowires for human motion detection and healthcare monitoring. *ACS Appl. Nano Mater.* **6**, 8772–8783 (2023). <https://doi.org/10.1021/acsanm.3c01153>
27. Q. Tian, W.R. Yan, Y.Q. Li, D. Ho, Bean pod-inspired ultrasensitive and self-healing pressure sensor based on laser-induced graphene and polystyrene microsphere sandwiched structure. *ACS Appl. Mater. Interfaces* **12**, 9710–9717 (2020). <https://doi.org/10.1021/acsami.9b18873>
28. M. Liu, J.N. Wu, H.Y. Cheng, Effects of laser processing parameters on properties of laser-induced graphene by irradiating  $\text{CO}_2$  laser on polyimide. *Sci. China Technol. Sci.* **65**, 41–52 (2022)

29. A.F. Carvalho, A.J.S. Fernandes, C. Leitao, J. Deuermeier, A.C. Marques, R. Martins, E. Fortunato, F.M. Costa, Laser-induced graphene strain sensors produced by ultraviolet irradiation of polyimide. *Adv. Funct. Mater.* **28**, 1805271 (2018). <https://doi.org/10.1002/adfm.201805271>
30. Y.Y. Lu, D.P. Kong, G. Yang, R.H. Wang, G.Y. Pang, H.Y. Luo, H.Y. Yang, K.C. Xu, Machine learning-enabled tactile sensor design for dynamic touch decoding. *Adv. Sci.* **10**, 2303949 (2023). <https://doi.org/10.1002/advs.202303949>
31. M. Zhong, S.C. Li, Y. Zou, H.Y. Fan, Y. Jiang, C. Qiu, J.L. Luo, L. Yang, hydrophobic surface array structure based on laser-induced graphene for deicing and anti-icing applications. *Micromachines-basel* **15**, 285 (2024). <https://doi.org/10.3390/mi15020285>
32. Y.W. Ma, Q. He, Preparation of superhydrophobic conductive CNT/PDMS film on paper by foam spraying method. *Colloid Surface A* **648**, 129327 (2022). <https://doi.org/10.1016/j.colsurfa.2022.129327>
33. X.T. Li, H.G. Liu, C.J. Gu, J.J. Zhang, T. Jiang, PDMS/TiO<sub>2</sub>/Ag hybrid substrate with intrinsic signal and clean surface for recyclable and quantitative SERS sensing. *Sen. Actuators B Chem.* **351**, 130886 (2022). <https://doi.org/10.1016/j.snb.2021.130886>
34. D.T.N. Rathnayake, N. Malik, S. Milone, S.A. Morion, Y.S. Guo, Interference effects in micro-Raman spectroscopy enable mapping of chemical gradients on an elastomer surface. *J. Phys. Chem. Lett.* **15**, 8467–8476 (2024). <https://doi.org/10.1021/acs.jpclett.4c01620>
35. D.Q. Ruan, G.Z. Chen, X.Z. Luo, L. Cheng, H.P. Wu, A.P. Liu, Bionic octopus-like flexible three-dimensional force sensor for meticulous handwriting recognition in human-computer interactions. *Nano Energy* **123**, 109357 (2024). <https://doi.org/10.1016/j.nanoen.2024.109357>
36. C.Y. Park, D.H. Seo, S.J. Lee, H.C. Kim, I.H. Lee, Characteristics of flexible pressure sensor according to circuit configuration of MWCNTs/polydimethylsiloxane composite and conductive layer. *Int J Precis Eng Man* **25**, 819–827 (2024)
37. K. Sinha, L.J. Meng, Q.W. Xu, X.H. Wang, Laser induction of graphene onto lignin-upgraded flexible polymer matrix. *Mater. Lett.* **286**, 129268 (2021). <https://doi.org/10.1016/j.matlet.2020.129268>
38. M.J. Cheok, Z. Omar, M.H. Jaward, A review of hand gesture and sign language recognition techniques. *Int J Mach Learn Cyb* **10**, 131–153 (2019)
39. M.M. Balaha, S. El-Kady, H.M. Balaha, M. Salama, E. Emad, M. Hassan, M.M. Saafan, A vision-based deep learning approach for independent-users Arabic sign language interpretation. *Multimed Tools Appl* **82**, 6807–6826 (2023)
40. L.S. Jia, X.Z. Zhou, C.Q. Xue, Non-trajectory-based gesture recognition in human-computer interaction based on hand skeleton data. *Multimed Tools Appl* **81**, 20509–20539 (2022)
41. L. Guo, Z.X. Lu, L.G. Yao, Human-machine interaction sensing technology based on hand gesture recognition: a review. *IEEE T Hum-Mach Syst* **51**, 300–309 (2021). <https://doi.org/10.1109/THMS.2021.3086003>
42. S.M. Zou, L.Q. Tao, G.Y. Wang, C.C. Zhu, Z.R. Peng, H. Sun, Y.B. Li, Y.G. Wei, T.L. Ren, Humidity-based human-machine interaction system for healthcare applications. *ACS Appl. Mater. Interfaces* **14**, 12606–12616 (2022). <https://doi.org/10.1021/acsami.1c23725>

Springer Nature or its licensor (e.g. a society or other partner) holds exclusive rights to this article under a publishing agreement with the author(s) or other rightsholder(s); author self-archiving of the accepted manuscript version of this article is solely governed by the terms of such publishing agreement and applicable law.